EVALUATION OF PILE RESPONSE TO LIQUEFACTION-INDUCED LATERAL SPREAD

by

T. D. O'Rourke[1]
W. D. Meyersohn[2]
Y. Shiba[3]
D. Chaudhuri[4]

ABSTRACT

This paper presents the results of a comprehensive analytical study of pile foundation response to lateral spread Analyses were performed with the computer code B-STRUCT, which has been shown to provide results which compare favorably with field observations of pile deformation under ground failure conditions Analytical results are combined to develop dimensionless plots which allow for the determination of failure mechanisms on the basis of relative stiffness and applied axial load For the first time, these results show quantitatively how the behavior of deep foundations changes as the ground alters its force-displacement characteristics from a soil-like to a fluid-like medium Dimensionless plots also are developed to determine surface soil displacement required to induce the formation of a plastic hinge under excessive bending conditions.

[1]Professor, School of Civil & Environmental Engineering, Cornell University, Ithaca, NY
[2]Staff Engineer, Dames and Moore, 221 Main Street, Suite 600, San Francisco, CA
[3]Visiting Scientist, School of Civil & Environmental Engineering, Cornell University, Ithaca, NY
[4]Graduate Research Assistant, School of Civil & Environmental Engineering, Cornell University, Ithaca, NY

INTRODUCTION

The lateral movement of liquefied soil against single piles and pile groups is an important problem in the design of deep foundations for buildings and bridges constructed in seismically active areas As shown by Hamada, et al [1986], the lateral spreading of loose saturated sands caused substantial damage to isolated pile foundations during the 1964 Niigata earthquake Considerable work on modeling the interaction between piles and liquefied soil has been undertaken in response to the Niigata observations [e g , Miura and O'Rourke, 1991, Meyersohn, et al , 1992], with the result that analytical procedures now are available to evaluate and design deep foundations affected by liquefaction-induced lateral spread

This paper describes an analytical approach for assessing pile and pile group response to large ground deformation caused by liquefaction Models for pile and liquefied soil behavior are embodied in a computer code, B-STRUCT, developed at Cornell University as a result of cooperative U S and Japanese research The paper explains the general characteristics of the analytical procedures, and describes the models adopted to represent the material nonlinearities of reinforced concrete Analytical results are compared with both laboratory test data and measured pile response to lateral spreads The failure modes of piles subjected to lateral spread are discussed, and the results of parametric studies are summarized to show how soil properties and subsurface geometry affect the axial load-carrying capacity of a pile and its lateral deformation

ANALYTICAL APPROACH

The analytical approach adopted for the assessment of soil-pile interaction is illustrated in Figure 1 The analytical approach is explained in detail elsewhere [Meyersohn, 1994, Meyersohn, et al , 1992], and only the salient features are described in this paper

The water table in Figure 1 is at the top of a liquefiable stratum of thickness, H_L, above which is the nonliquefiable soil cover, L_L The pile is embedded at a distance, L_b, into a firm, nonliquefiable base Soil displacements are applied in a series of load increments until the maximum soil displacement at ground surface, d_h, is achieved Any distribution of soil displacement can be simulated For purposes of illustration, a trapezoidal distribution is applied in the figure Axial load, shear, and moment can be specified at the top of the pile

The B-STRUCT program models the pile foundation by a series of beam elements, while the surrounding soil is modeled by means of transverse and longitudinal bilinear spring-slider elements Although the diagram shows only springs offering lateral resistance, the program accounts for the effects of skin friction and adhesion as well

Each beam element is formulated as a nonlinear elastic member, with material nonlinearities concentrated at nodal points An updated Lagrangian formulation is used to account for geometric nonlinearities in the simulation of large deformation A solution algorithm, based on the modified

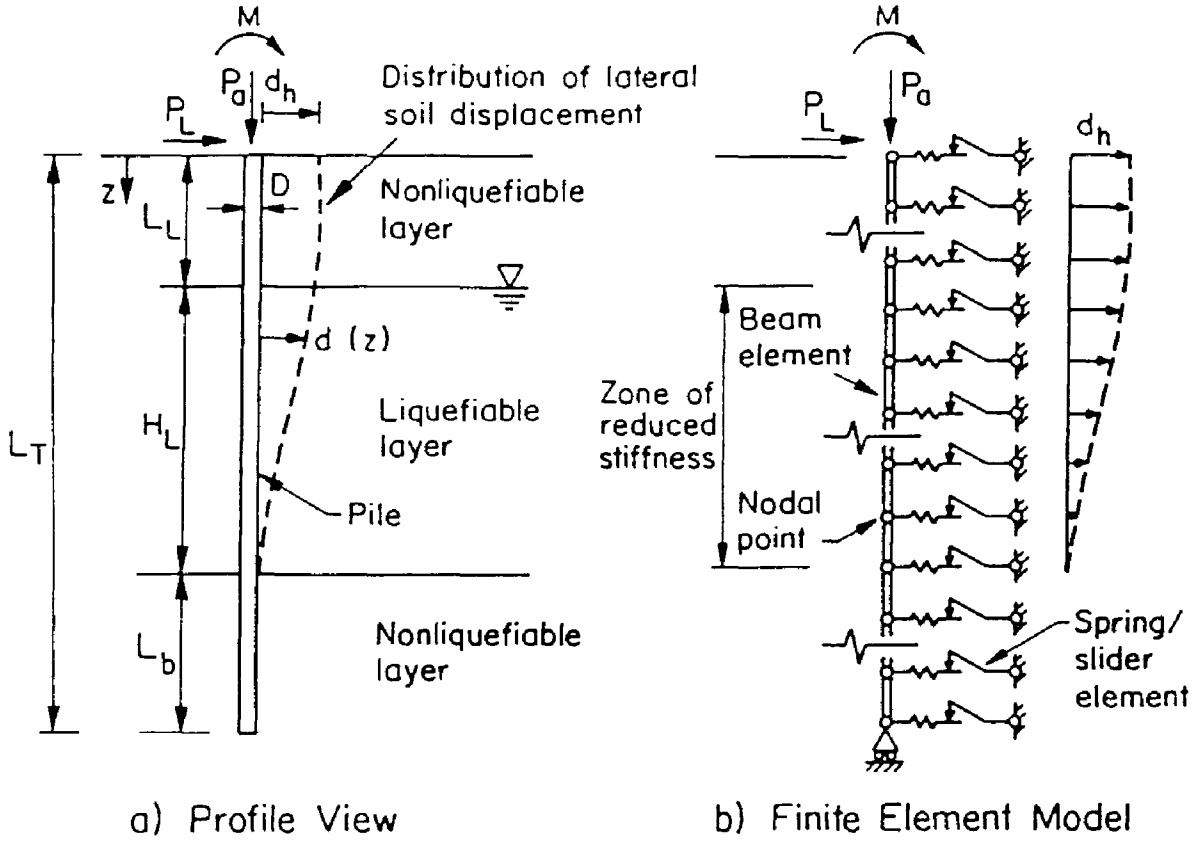

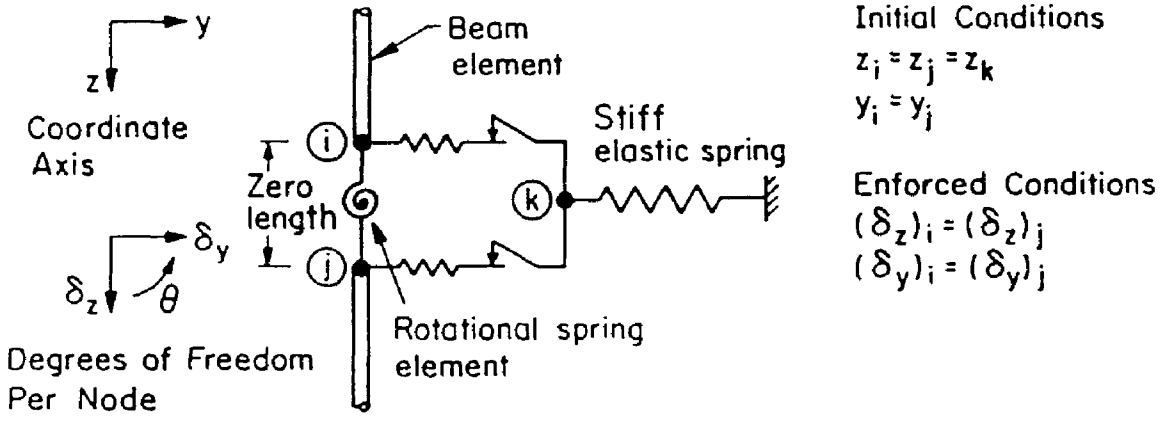

FIGURE 1. Analytical Model for the Soil-Pile System

Newton-Raphson method with a mixed-step iteration technique, is used for convergence Beam elements are formulated with the capability of detecting buckling states

Because the mechanical behavior of liquefied soil is complex and imprecisely understood, a relatively simple procedure has been adopted to account for soil strength and stiffness. The choice of a simple interaction mechanism permits the evaluation of important trends and influential parameters, without introducing undue complexity in the formulation of the problem. As will be shown in a forthcoming section of this paper, the simple model adopted herein leads to analytical results which compare very favorably with observed earthquake performance

The soil yielding force, p_u, is determined from lateral bearing capacity factors proposed by Hansen [1961]. The soil spring stiffness is determined from the coefficient of horizontal subgrade reaction, k_h, proposed by Terzaghi [1955], which is given by the expression.

$$k_h = n_h \frac{z}{D} \tag{1}$$

in which n_h is the constant of horizontal subgrade reaction, z is the depth, and D is the pile diameter. The yielding spring displacement was determined by dividing the yielding force by the spring stiffness Stiffness and yielding force reduction due to liquefaction are accomplished by dividing k_h and p_u, respectively, by a reduction factor, R_f, larger than 1 The spacing of the spring-slider elements was chosen to conform with the maximum spacing required for beam on elastic foundation analysis [i e., Boresi, et al., 1978]

Nonlinear flexural behavior of the pile material is accounted for by means of rotational springs, which utilize nonlinear moment-rotation laws The rotational springs, which connect individual beam elements, are used to represent cracking and ultimate flexural states of reinforced concrete piles Figure 1c illustrates a typical beam element-rotational spring connection A zero-length rotational spring is placed between adjacent beam elements A condition is enforced in which both axial and transverse displacements of nodes i and j are the same

Since the material nonlinearity of the model is concentrated at the rotational springs, the lateral deflection of the pile is the combined result of elastic bending of the beam elements and nonlinear rotation of the connecting rotational springs On the basis of modeling techniques proposed by Miura and O'Rourke [1991], the relation between moment and curvature of the pile is converted into a relation between moment and rotation of the rotational spring elements

ANALYTICAL MODELING OF REINFORCED CONCRETE

Figure 2 illustrates the cross-section, as well as the strain and stress distribution, in the concrete of a circular reinforced pile The axial load acting on the cross-section is assumed to be constant and equal to P_a The combined action of applied axial load and bending moment causes the pile to bend and crack The resulting strain distribution in both concrete and steel is presented in the figure The depth of the neutral axis, c, indicates the extent of the compressed portion of the pile

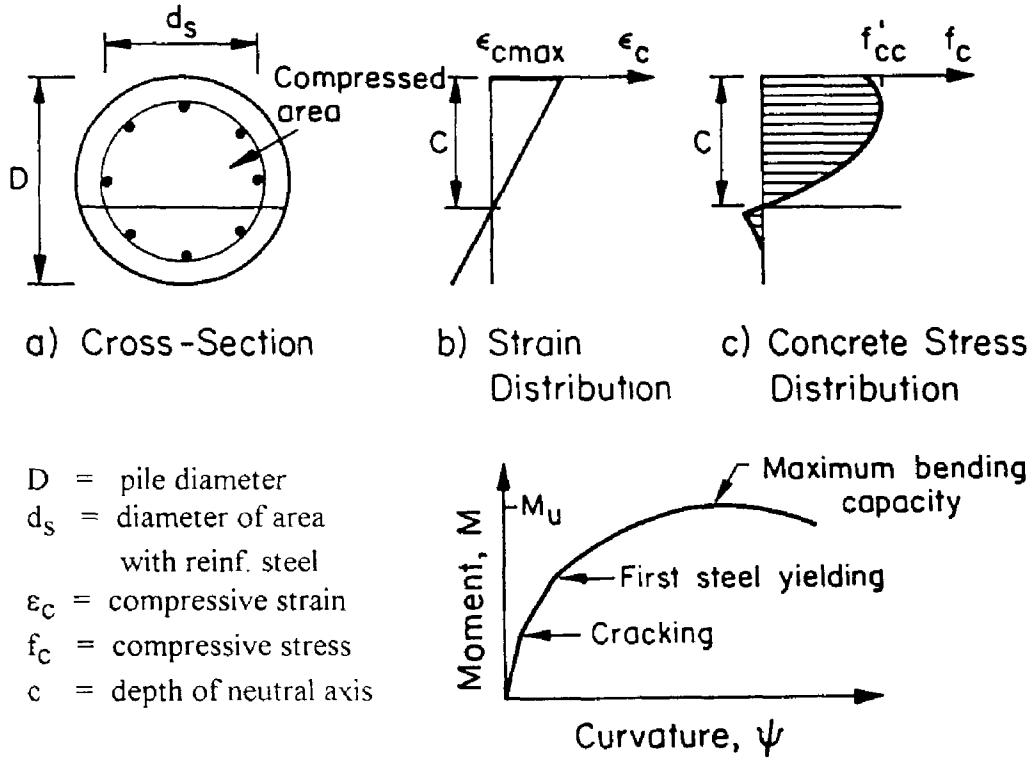

FIGURE 2. Cross-Section, Strain, and Stress Distribution for Theoretical Calculation of Moment-Curvature Relationships for Reinforced Concrete Sections

Concrete stresses are determined from the linear distribution of strain within the compressed area of the pile

To calculate the theoretical moment-curvature relationship for a given axial load, a value of maximum compressive strain in the extreme fiber, ε_{cmax}, is specified Then an iterative procedure is performed to determine the neutral axis depth at which the resulting internal forces balance the externally applied axial load and moment In this process, for an assumed value of c, the strain distribution in the section can be determined The resulting concrete force and its position, as well as the steel reinforcement loads, are calculated

If the total resisting force does not balance the external axial load, the depth of the neutral axis is changed and the process is repeated When the error between internal and external forces is less than a specified tolerance, typically 0 01%, the resulting moment of the internal forces with respect to the center of the section is that being resisted by the pile The curvature associated with that moment is calculated as the ratio between the maximum concrete strain and the distance to the neutral axis, c

The maximum bending capacity of concrete piles usually is achieved at maximum concrete compressive strains of 0 003 to 0 0035 [e g , Kent and Park, 1971] In this work, moment-curvature determinations were carried to a maximum concrete strain of 0 0035

Bending test data were obtained from quality control tests performed on production piles fabricated by Daido Concrete Co , Ltd , of Japan The Daido Concrete Co produces both reinforced and prestressed concrete piles by centrifuge, or spun, processing Data for 400-mm-diameter, 8-m-long piles were provided The piles either were reinforced concrete piles (RC) with a wall thickness of 70 mm, or prestressed concrete piles (PHC) with a wall thickness of 65 mm Material properties and pile geometries, as well as details of the analytical modeling, are described by Meyersohn [1994] All piles were tested in pure bending without axial load Figure 3 illustrates the general test set-up Piles were placed on supports 4 8 m apart A transverse load was applied such that an approximately constant moment region occurred in the middle of the pile

Moment-curvature relationships for each pile were calculated using the stress-strain curve for confined concrete in compression proposed by Mander, et al [1988] Tensile stiffening of reinforced concrete piles was modeled as the linear falling branch of Mier [1987], while that of prestressed concrete piles was determined according to the model of Marzouk and Chen [1993]

If the analytical moment-curvature relationship is correct, the estimation of displacements from this relationship should give the correct pile deflections From the bending moment distribution, which includes the actions of both self-weight and external load, the curvature distribution along the test specimen was determined from the moment-curvature relationship Then, the integration of curvature was used to calculate deflections along the pile

Figure 4 shows comparisons between the analytical and measured load-displacement plots The agreement in both cases is excellent Initial cracking of the reinforced concrete specimen is evinced by a sharp change in slope at low levels of externally applied load Cracking also is successfully predicted by the analytical model Curves for the prestressed concrete specimen change in slope at a load of about 95 kN This load corresponds, approximately, to the development of full cracking, which occurs once all contribution from tension stiffening has disappeared After cracking develops, the experimental load-displacement curve shows a quasi-linear trend in parallel with the analytical results

COMPARISON OF FIELD OBSERVATIONS AND ANALYTICAL RESULTS

Detailed measurements of reinforced concrete pile deformation caused by lateral spread at the NHK and Niigata Family Courthouse (NFCH) Buildings in Niigata have been reported by Hamada [1992] Analytical studies of the NHK Building foundations have been published and discussed elsewhere [e g , Miura and O'Rourke, 1991, Meyersohn, et al , 1992] In this work, attention will be focused on the NFCH Building

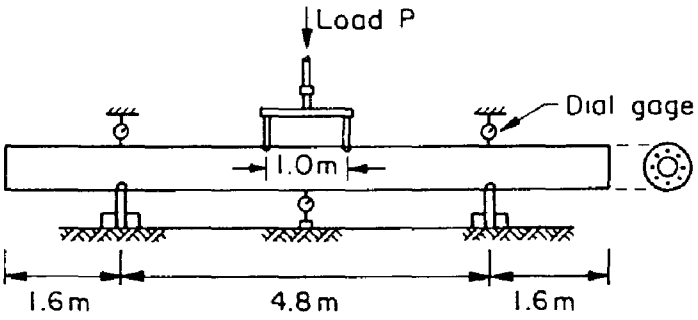

FIGURE 3. Set-Up Test for Daido Concrete Pile Specimens

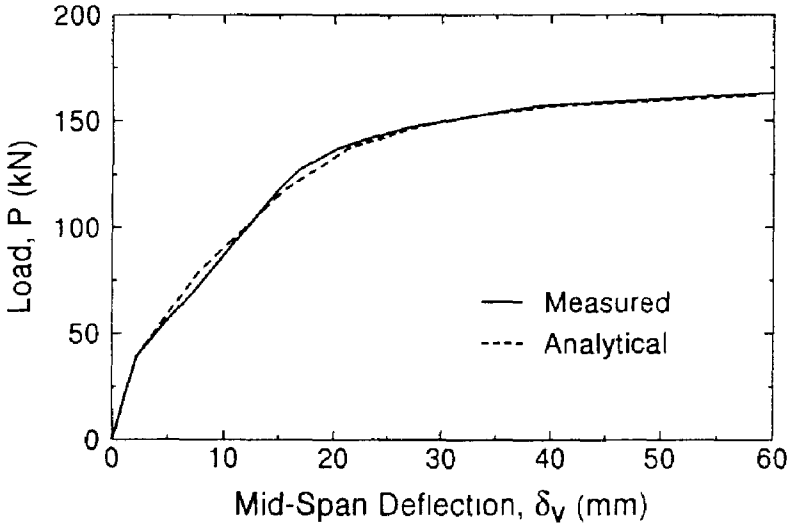

a) Reinforced Concrete Pile

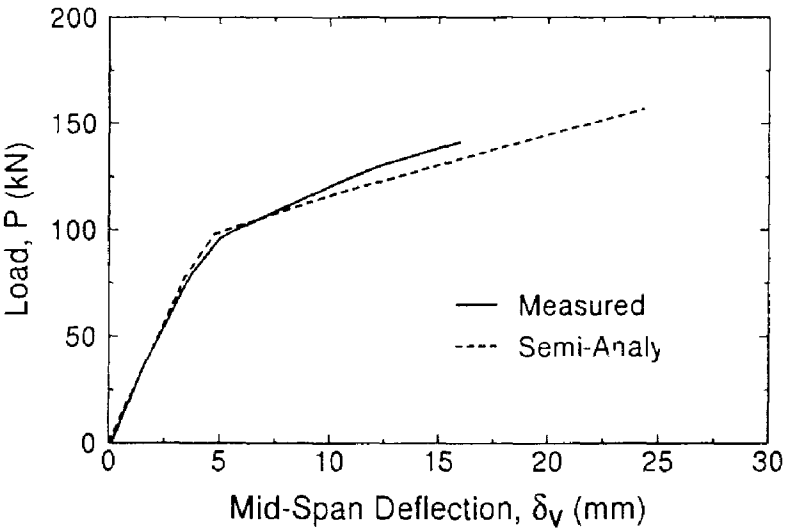

b) Prestressed Concrete Pile

FIGURE 4. Comparison of Analytical and Measured Load Displacement Plots

The NFCH Building was a three-story reinforced concrete structure founded on reinforced concrete piles. As a result of lateral spread during the 1964 Niigata earthquake, the building displaced horizontally approximately 0 5 to 1.5 m, according to photogrametic studies performed by Yoshida and Hamada [1991]

As explained by Meyersohn, et al. [1992], two 350-mm-diameter piles, referred to as Piles 1 and 2, were carefully excavated and examined. Each supported a small footing. Figure 5 shows a scale diagram of the damage state of each pile, along with the measured SPT values. The piles were separated from each other in the field by about 24 m. The uncorrected SPT values are mostly less than 10 for depths up to 8 m, but sharply increase at greater depths. The water table is located at a depth of 1 70 m, however, that value was measured 25 years after the earthquake [Hamada, 1992]

Pile 1 did not reach the lower interface, whereas Pile 2 penetrated into the lower nonliquefied soil. Both piles were damaged at about 2 m from the ground surface, which roughly coincides with the upper interface between liquefied and nonliquefied soil At this location, Pile 1 showed bending cracks, while Pile 2 showed a severe shear dislocation of about 180 mm In addition, severe bending cracks at depths between 6 5 and 8 5 m were observed in Pile 2

Deflection values were obtained for Piles 1 and 2 along their lengths Pile 1 was "dragged" into its deflected shape by liquefied soil Its deformation was related to the forces conveyed by liquefied soil and the relative soil/pile stiffness, both of which depend on R_f By iterative analyses, therefore, a value of R_f was identified which results in the most favorable comparison between predicted and observed deformations If this value of R_f also results in a suitable match between the prediction and measurement of Pile 2 deformation, then the value of R_f so chosen should provide a reliable measure of the average stiffness reduction experienced by the liquefied soil

The soil profile and displacement pattern for Pile 1 are presented in Figure 6a The maximum soil displacement at the ground surface, d_h, was taken as 0 66 m, which is equal to the measured offset in the pile An explanation of the modeling assumptions and procedures is given by Meyersohn [1994]

Figure 6b plots the ratio between calculated and measured pile offset as a function of R_f for a maximum surface soil displacement of 0 66 m. Measured and calculated offsets agree for R_f = 60, which may be regarded as representative of the state of the liquefiable soil at the site

Results of the analyses for Pile 1 with R_f = 60 are presented in Figure 7, which shows pile deflections and bending moments at different stages of soil displacement Superimposed are the measurements of transverse deflections obtained by Yoshida and Hamada [1991] from the excavated pile Pile 1 develops a plastic hinge at the upper interface between the liquefiable and overlying soil when displacement reaches a magnitude of about 0 54 m With additional soil displacement, the angle formed at the plastic hinge increases. When the surface soil displacement reaches the maximum specified value of 0 66 m, the observed deflected shape of the pile agrees closely with the analytical deformation pattern The bending moment diagrams indicate that very little redistribution of moment occurs after hinge formation

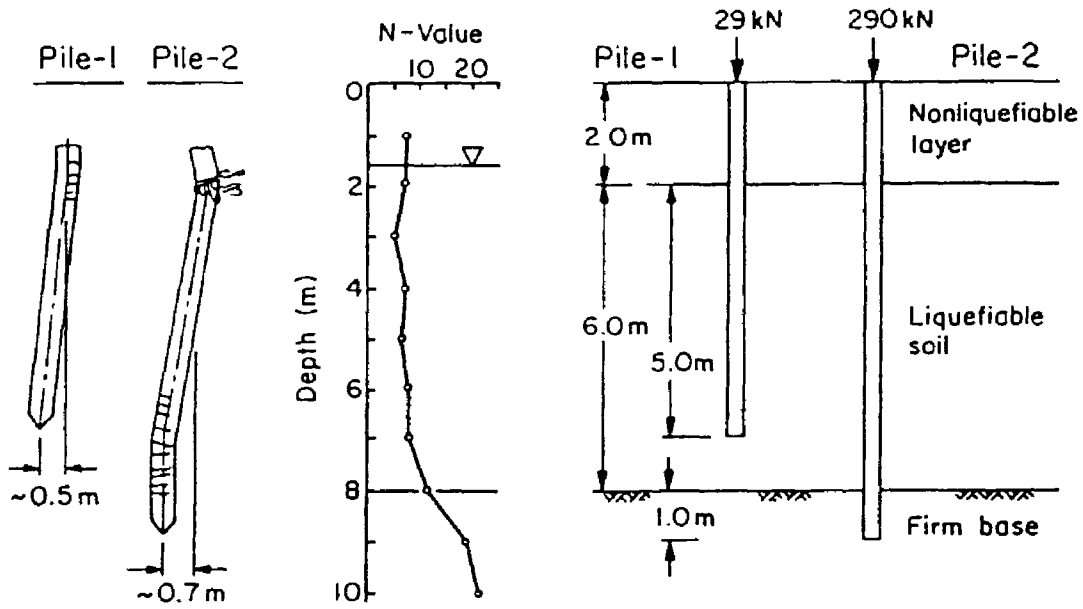

FIGURE 5. Observed Pile Deformation and Soil Conditions at NFCH Building

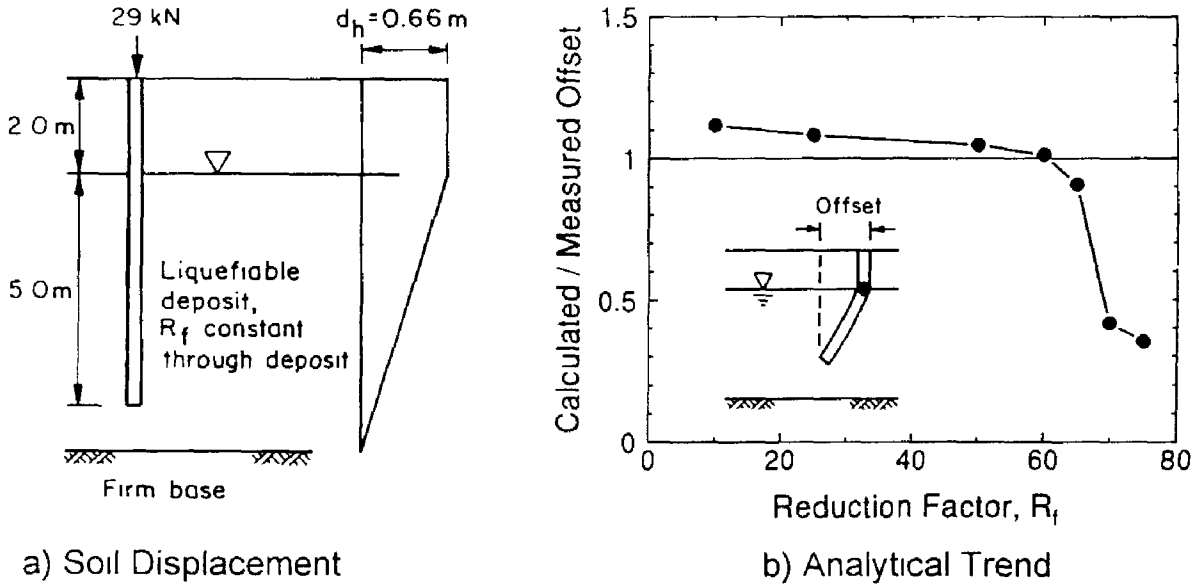

FIGURE 6. Soil Displacement Pattern and Ratio of Calculated to Measured Offset as a Function of R_f

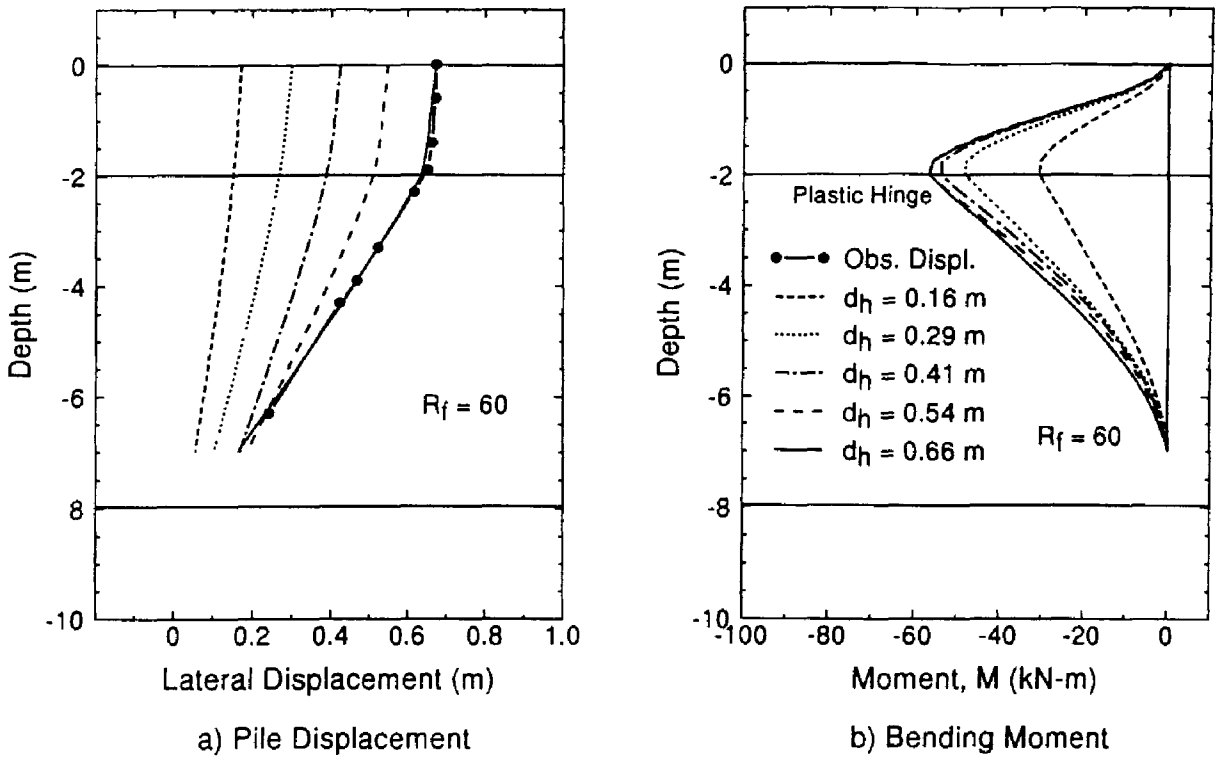

FIGURE 7. Analytical Results for Pile 1 at the NFCH Building

An examination of the measured shape and photographs provided by Yoshida and Hamada [1991] indicates that the failure at the lower end of Pile 2 was distributed over its bottom 2 m The absence of a sharp kink at this location suggests that the soil offered higher lateral resistance than the liquefied soil above, limiting in this way pile deflections

In the analysis of Pile 2, liquefaction was assumed between the depths of 2 0 and 7 0 m, thereby resulting in the soil displacement profile shown in Figure 8 A R_f of 60 was assigned to the soil profile between 2 0 and 7 0 m Between the depths of 7 0 and 8 0 m, the value of R_f was taken as 1

Numerical results are presented in Figure 9, which shows pile lateral deflections and bending moments at various stages of soil displacement Numerical results indicate that plastic hinge formation occurs first at the lower interface, when the surface soil displacement is about 0 24 m A second hinge develops at the upper interface at a soil displacement of about 0 32 m

The agreement between measured and analytical deformations is good If it is assumed that upper plastic hinge formation weakened the pile, thereby contributing to shear offset at this location, the analytical results for a 0 66 m soil displacement compare very favorably with observed deforma-

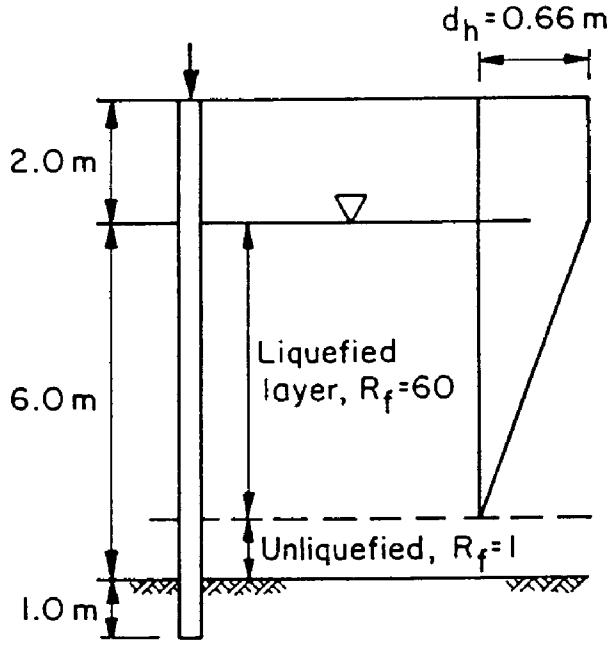

FIGURE 8. Simplified Soil Profile and Assumed Soil Displacement Pattern for Pile 2 at the NFCH Building

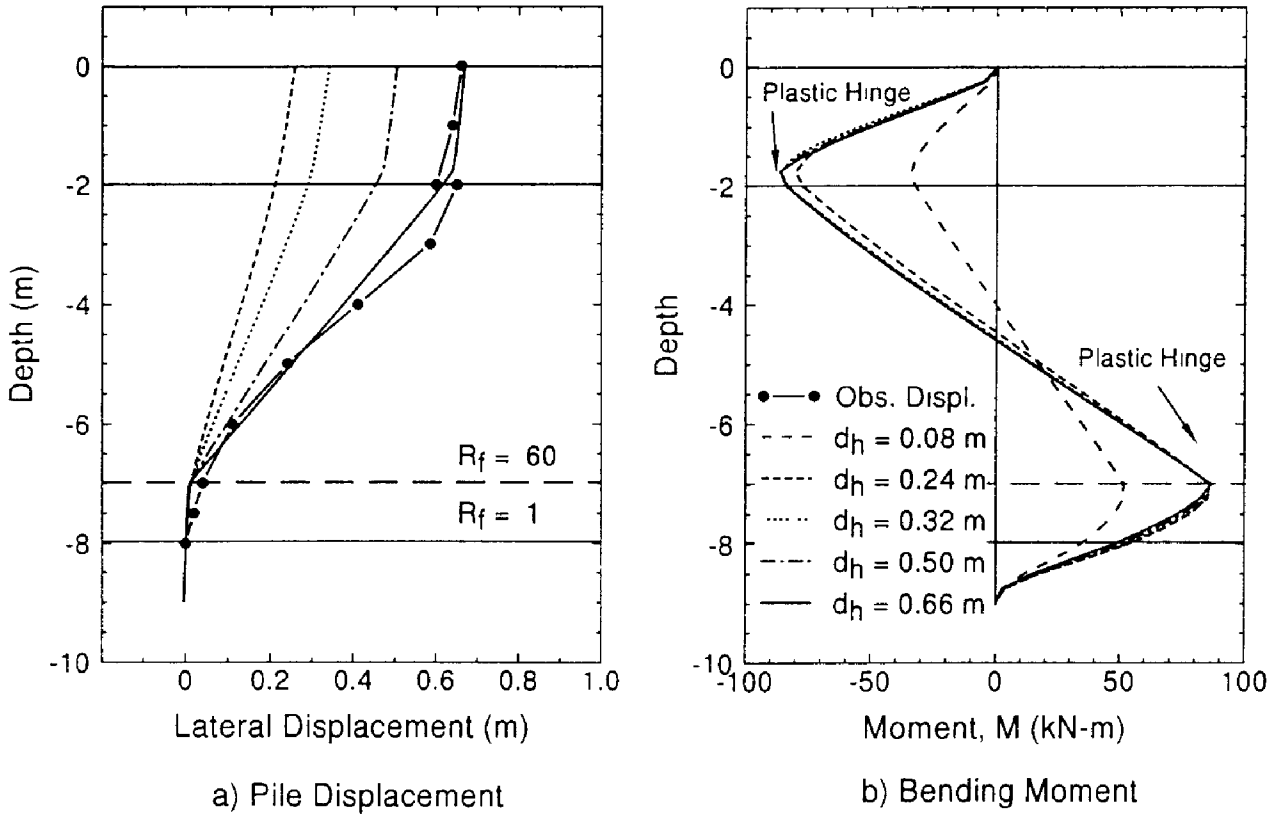

a) Pile Displacement

b) Bending Moment

FIGURE 9. Analytical Results for Pile 2 at the NFCH Building

tion In this case, hinge formation would have been followed by shear failure, leading to the observed relative movement between the head and underlying body of the pile.

FAILURE MODES AND DEFORMATION CHARACTERISTICS

Two distinctive failure modes can be recognized in piles subjected to lateral spreads resulting from soil liquefaction. In the first one, lateral pile deflections induced by horizontal soil displacement may result in the pile reaching its bending capacity, thus developing a plastic hinge On the other hand, the lack of sufficient lateral support due to the reduced stiffness of the liquefied soil and the lateral deflection imposed on the pile, may result in buckling

Figure 10 illustrates the possible failure mechanisms The depth to water table in the diagrams simply indicates the possible extent of an upper nonliquefied layer. Buckling and plastic hinge formation are shown in Figures 10 a and b, respectively. Whether the bending capacity of the pile is first reached in the vicinity of the upper or the lower interface depends on the amount of lateral restraint offered by the nonliquefied soil In general, hinge formation will tend to occur at the lower interface, since the higher confining effective stress at a greater depth results in larger lateral resistance than at a shallower depth (Figure 10b)

A third type of failure is illustrated in Figure 10c It involves excessive rigid body rotation of the pile, which is a characteristic of large diameter piles and piers This type of response to lateral soil displacement arises primarily from a lack of sufficient restraint at the bottom of the pile, either due to an inadequate imbedment length or to low resistance of the foundation material against lateral movement With increasing soil movement, this form of pile response may be followed by the formation of a plastic hinge at the lower interface, or by a premature collapse of the foundation due to a combination of excessive rotation and lack of lateral support

Another behavioral mode is soil flow, which is characterized by flow of liquefied soil around the pile It usually is associated with stiff foundations, such as large diameter piles, piers, and groups of closely spaced piles Under these conditions, a relatively stiff pile will flex until the soil has mobilized its full resistance against the pile Additional soil movement occurs as a flow relative to the pile This form of response may not lead necessarily to pile failure, since soil will displace without causing additional pile deflection

B-STRUCT accounts for the effects of geometric nonlinearities, that is to say, it performs a second-order analysis The coupled action of axial load effects and geometric nonlinearities enables the program, in certain cases, to achieve convergence in a post-buckling analysis.

PARAMETRIC STUDY OF ACCEPTABLE AXIAL LOAD

Parametric studies were performed [Meyersohn, 1994] to develop two sets of dimensionless

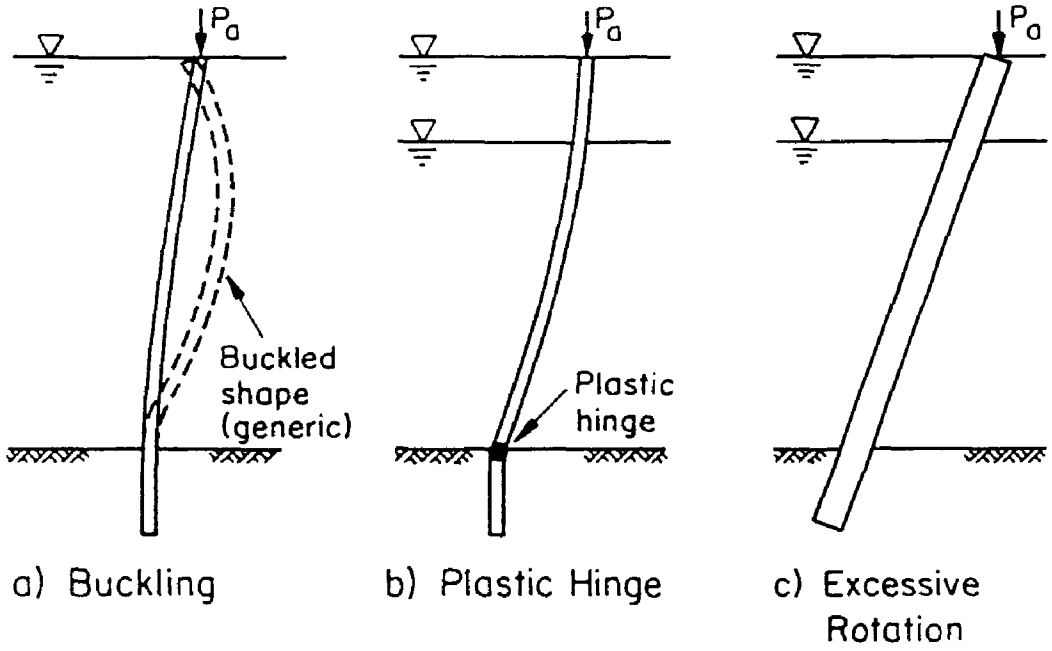

FIGURE 10. Pile Failure Modes

curves, which provide for 1) the determination of acceptable levels of axial load that do not result in pile buckling, and 2) the maximum lateral soil movement at which excessive pile flexure occurs, given that axial load is below the buckling limit As an illustration of typical results obtained in the parametric study, Figure 11 summarizes the analytical trends for the 350-mm-diameter pile The inset in the figure shows the conditions associated with the analyses the water table is at the ground surface with a total thickness of liquefied soil of 8 5 m The figure plots surface ground displacements as a function of applied axial force for different values of R_f. The soil displacement in the vertical axis denotes the displacement at which the pile either buckles or develops a plastic hinge

The abrupt change of slope in curves associated with R_f values of 10, 50, and 100 indicates a transition load, P_t, which is the axial load at which the pile buckles simultaneously as it develops a plastic hinge At axial loads smaller than P_t, the pile fails by excessive bending, while at higher loads, the pile buckles Note that, as the axial load increases above P_t, the soil displacement, d_h, decreases significantly The transition load increases as R_f decreases because the increased soil stiffness provides additional lateral support against buckling

As the stiffness and strength of the soil decrease as a result of liquefaction, lateral pile confinement also decreases, which tends to induce buckling at lower axial loads As the degree of lique-

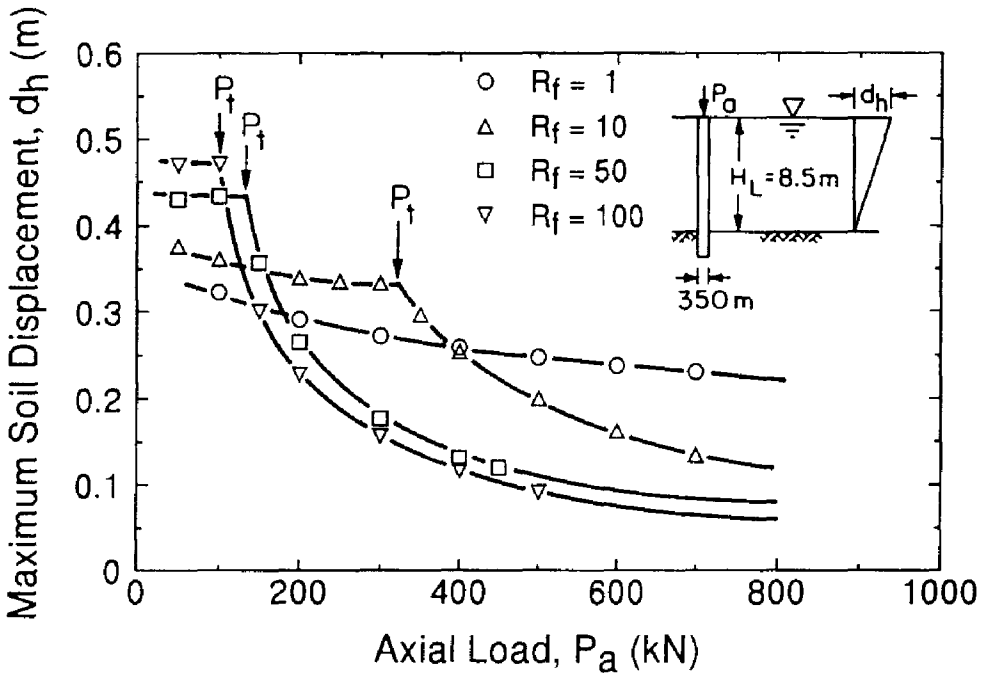

FIGURE 11. Maximum Soil Displacement versus Axial Load for a 350-mm-Diameter Pile, H_L = 8 5 m, L_b = 2 5 m, L_L = 0 0 m

faction becomes more severe. however, its stiffness eventually decreases to a state in which the buckling capacity begins to increase because the liquefied soil movement cannot impose additional pile deflections Under these conditions, the soil flows relative to the pile, and buckling capacity increases

These two opposing trends are illustrated schematically in Figure 12, in which the axial load is plotted as a function of the relative stiffness between soil and pile For illustration purposes, the relative stiffness between the soil and the pile is expressed as the ratio between the modulus of lateral subgrade reaction of liquefied soil, k_{hl}, and the bending stiffness of the pile, EI The two straight lines in the figure separate stable from unstable states Line AB defines the boundary for soil flow between stable conditions and buckling, while line BC defines the boundary between potential bending failure and buckling

An axial load along line AB, which divides soil flow from pile buckling states, is referred to in this work as the flow load, P_f A load lying along line BC is called the transition load, P_t In the absence of soil, the relative stiffness between soil and pile is zero For these conditions, point A in Figure 12 should be equal to the Euler buckling load, provided the pile is restrained fully against rotation at the bottom of the liquefied layer

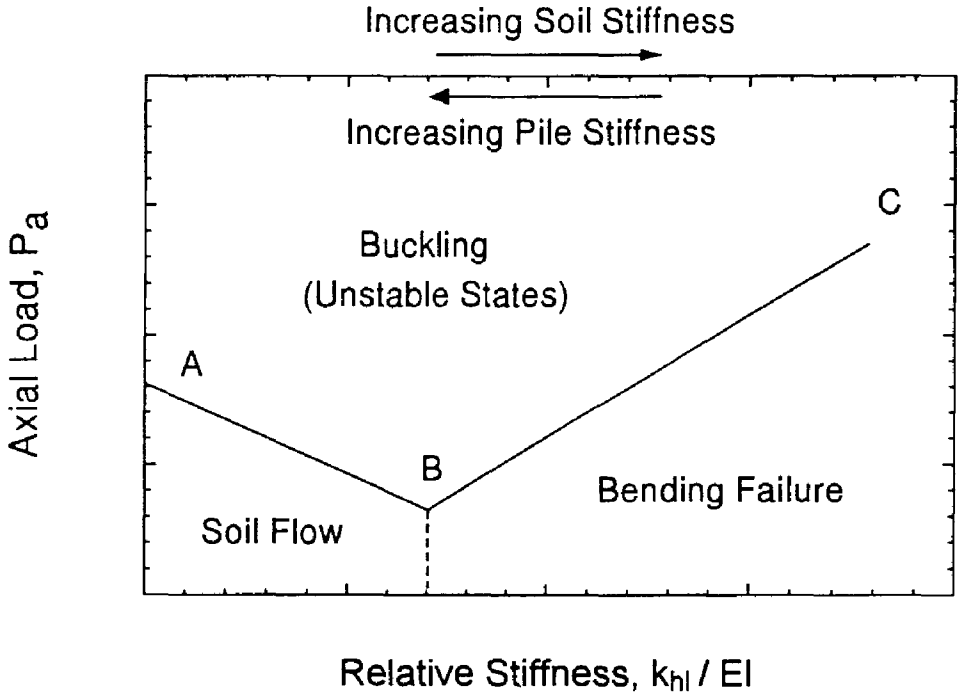

FIGURE 12. Failure States of Piles Subjected to Lateral Spread

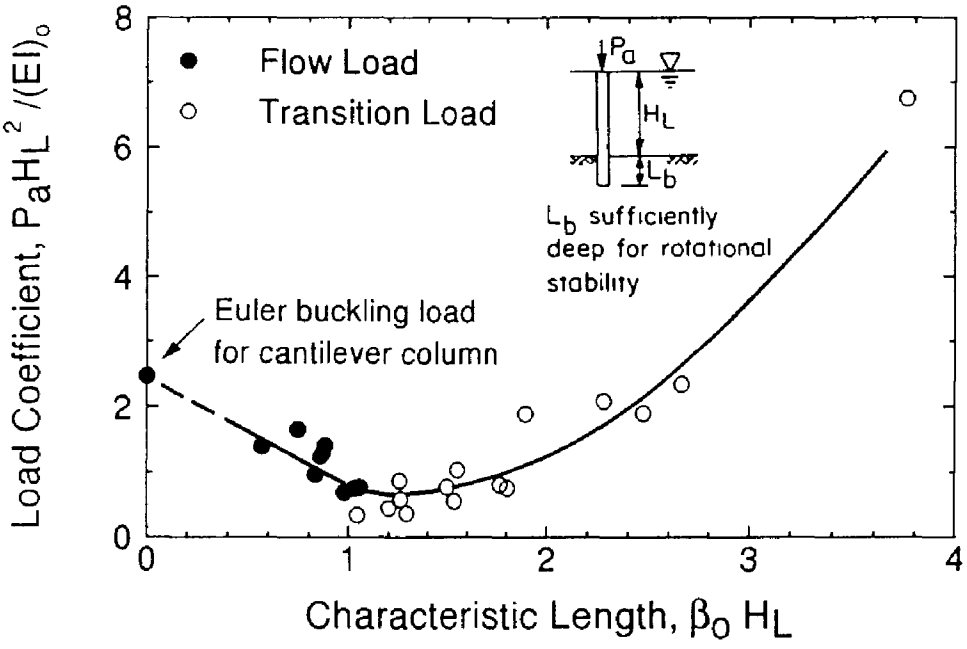

FIGURE 13. Analytical Results for Flow and Transition Loads, L_L = 0 0 m

The ability to predict the potential for buckling is of significant practical importance. If a pile develops a plastic hinge, or if the soil flows around it, the pile generally can accommodate more lateral soil displacement than if it were to buckle. To provide guidance for the problem, transition and flow loads were identified from the computer results and are plotted in Figure 13. In general, flow loads were associated almost exclusively with the condition in which the water table is at the ground surface and with reduction factors larger than about 50. Results in Figure 13 correspond to the case in which the water table is at the ground surface. The horizontal axis, $\beta_o H_L$, is a dimensionless number, referred to as the characteristic length, which depends on the flexural rigidity of the pile, as well as the stiffness of the soil. The parameter β_o is defined as:

$$\beta_o = \sqrt[4]{\frac{n_{hl} D}{(EI)_o}} \tag{2}$$

in which n_{hl} is the coefficient of horizontal subgrade reaction of the liquefied soil, D is the pile diameter, and $(EI)_o$ is the initial, uncracked stiffness of the reinforced concrete pile.

It should be recognized that, for liquefied soil, the coefficient of horizontal subgrade reaction will be obtained by dividing the value for intact soil by the reduction factor (i.e., $n_{hl} = n_h/R_f$) The value of $(EI)_o$ corresponds to the bending stiffness of the uncracked section of the pile, and can be determined by the expression

$$(EI)_o = \frac{M_c}{\psi_c} \tag{3}$$

in which M_c and ψ_c are the cracking moment and the cracking curvature, respectively

The axial load has been plotted as a dimensionless coefficient defined as

$$\frac{P_a H_L^2}{(EI)_o} \tag{4}$$

In Figure 13, open symbols indicate cases in which buckling occurred simultaneously with the formation of a plastic hinge Solid symbols denote cases of buckling caused by soil flow Numerical results indicate that the transition load increases, while the flow load decreases, as the characteristic length of the system increases. The observed scatter arises mainly as a result of the nonlinearities of the system that are not accounted for completely by the terms used to define both axes

Trends shown in Figure 13 agree with the conceptual framework of pile behavior presented in Figure 12 The characteristic length at which flow failure and bending failure occurs (point B in Figure 12) ranges from 1.0 to 1 1, with an average of 1 06 Since this point delineates the boundary between two different pile responses, the characteristic length associated with this limit will be referred to herein as the critical characteristic length, L_c

Hence, a soil-pile system with a value of L_c smaller than about 1 0 is a potential candidate to develop flow failure At higher characteristic lengths, soil flow can not occur and the pile will fail in bending Without soil, the characteristic length takes a value of zero and the flow load would be equal to the Euler critical load for a cantilever column perfectly embedded at the bottom of the liquefied layer The load coefficient associated with the critical Euler load of a cantilever column takes a value of $\pi^2/4$, or about 2 47

PARAMETRIC STUDY OF MAXIMUM SOIL DISPLACEMENT

If the axial load acting on the pile is of such magnitude that buckling will not occur, and if the characteristic length of the soil-pile system is such that flow failure can not develop, the next logical step is to assess the amount of soil displacement required to cause bending failure At the moment of bending failure, a large portion of the pile is in a post-cracked state Hence, a more representative characteristic length of the system can be defined on the basis of reduced pile stiffness The characteristic length of the cracked section, $\beta_\alpha H_L$, is expressed as

$$\beta_\alpha H_L = \sqrt[4]{\frac{n_{hl} D}{(EI)_\alpha}} H_L \tag{5}$$

in which $(EI)_\alpha$ is a secant bending stiffness, the value of which is illustrated with the aid of Figure 14 The value of $(EI)_\alpha$ is taken as the slope between the point of maximum bending capacity (M_u, ψ_u) and a point that results from the intersection between the initial slope line, $(EI)_o$, and a horizontal line drawn at a value of α times M_u Here α is a positive number less than 1 0 The value of α determines the slope of the secant stiffness It can be shown that $(EI)_\alpha$ is given by the expression

$$(EI)_\alpha = \frac{(1-\alpha)}{1-\frac{\alpha(EI)_u}{(EI)_o}} (EI)_u \tag{6}$$

in which $(EI)_u$ is simply M_u/ψ_u, the maximum moment divided by the maximum curvature at a concrete strain of 0 0035

Examination of numerical results indicates that a value of α equal to 0 70 represents a good measure of secant stiffness, which helps collapse numerical results into well defined trends Hence, α = 0 70 was used in the definition of the characteristic length of the cracked section in Equation 5

From the numerical results of the parametric study, soil displacements at bending failure were determined and are plotted in Figure 15 The horizontal axis is the normalized length $B_{70}H_L$, while

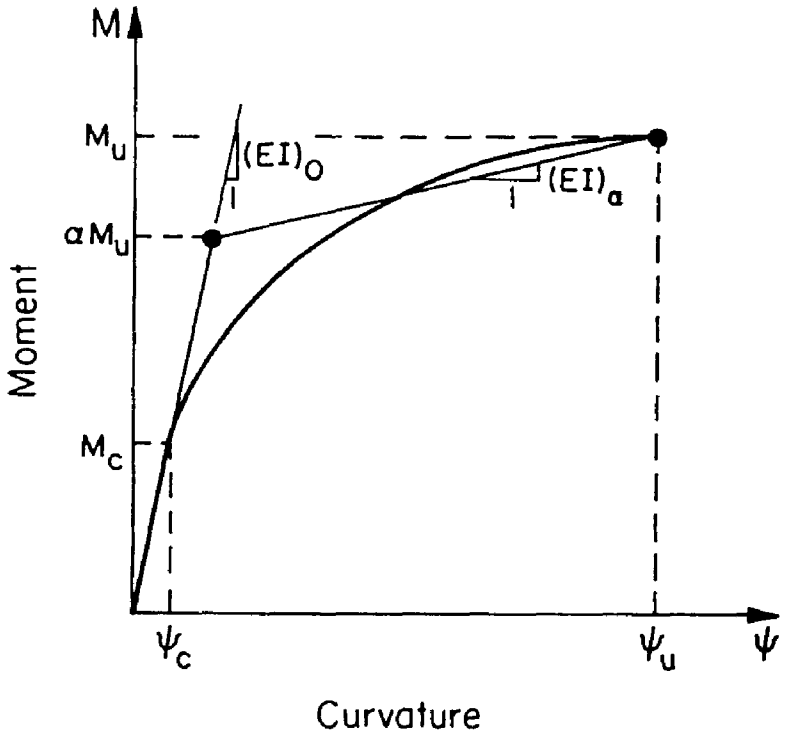

FIGURE 14. Definition of Secant Bending Stiffness, $(EI)_\alpha$

the vertical axis is given as a function of the dimensionless expression Δ_h, defined as

$$\Delta_h = \frac{d_h D}{H_L^2} \sqrt[4]{R_f} \tag{7}$$

The normalized soil displacement, Δ_h, is a measure of the average strain developed in the pile, as explained by Meyersohn, et al [1992]

Curves in Figure 15 were developed for axial loads less than the transition load, P_t, and generally equal to about one-fourth to one-third of the ultimate bearing capacity of the pile They represent a reasonable practical range of working loads that contribute to moments in the pile, and hence, to flexural failure under horizontal soil displacement As indicated in the figures, upper limits for the analytical trends are associated with 350-mm-diameter piles, while the lower limit defines Δ_h values associated with 1 0-m-diameter piles

As discussed in the preceding section, there exists a value of $\beta_o H_L$ that establishes the boundary between bending failure and soil flow, which is called the critical characteristic length of the soil-pile system, L_c These L_c values were calculated to be 1 06 and 0 68, for L_L of 0 0 and 1 5

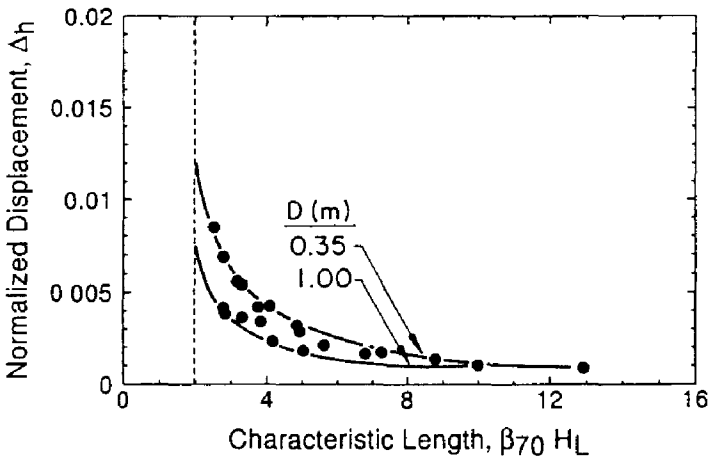

a) L_L = 0.0 m

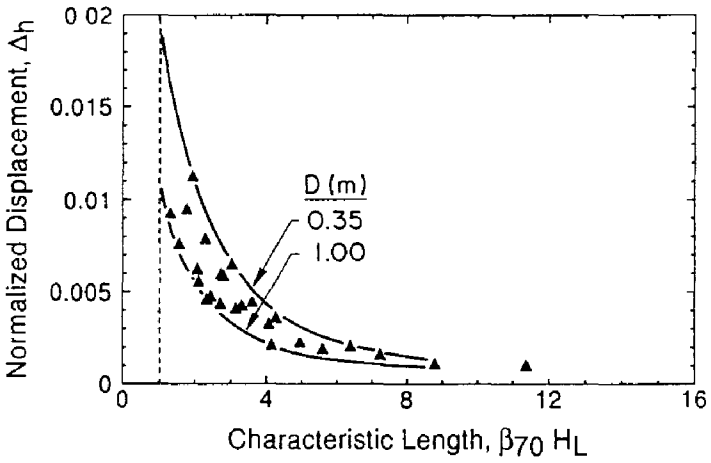

b) L_L = 1.5 m

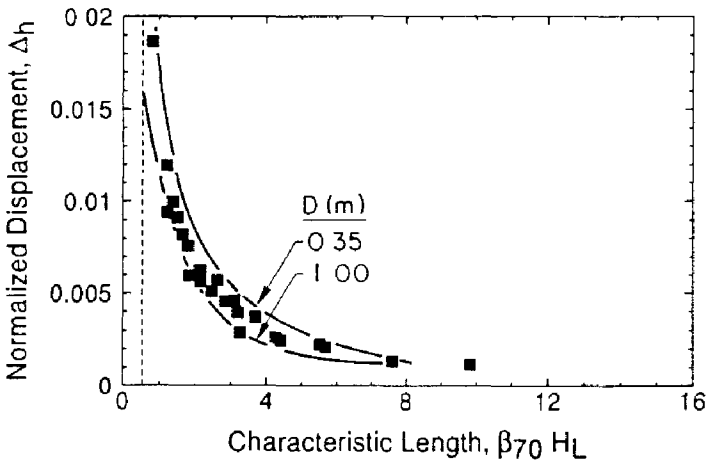

c) L_L = 3.0 m

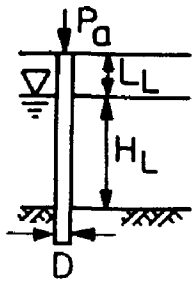

FIGURE 15. Normalized Soil Displacement versus Characteristic Length to Evaluate Lateral Spread Movement to Cause Bending Failure

m, respectively In terms of the new definition of the characteristic length, $\beta_{70}H_L$, there is a corresponding critical characteristic length, L_{c70} The differences in their numerical values arise because β_o and β_{70} are defined on the basis of a different characterization of the bending stiffness of the pile The ratio between $(EI)_o$ and $(EI)_{70}$ depends on the diameter of the pile and the axial load, and generally ranges between 5 and 100 Thus, the ratio between β_{70} and β_o normally would vary from 1 5 to 3.2, for the same H_L, with an average value of 2 An examination of $(EI)_{70}$ values associated with cases of flow failure reveals that L_{c70} is approximately equal to 2 0 and 1 0 for L_L equal to 0 0 and 1.5 m, respectively

Vertical dashed lines define the critical characteristic length, L_{c70}, below which there is flow failure It is apparent that all cases of bending failure plot to the right of the limiting lines. However, there is a tendency for the normalized displacement, Δ_h, to increase as $\beta_{70}H_L$ approaches the limiting line. This increase is consistent with the tendency of the soil to flow as the characteristic length of the system decreases

Figure 15 indicates a decrease in Δ_h as the characteristic length of the cracked section increases. A very flexible pile will have a larger characteristic length than a relatively stiff pile Since the flexible pile will try to conform to the soil displacement, large curvatures will develop near the interfaces between liquefied and intact soil The pile will, therefore, experience bending failure at a relatively low value of soil deformation A stiff pile will provide a greater resistance to soil displacement, allowing for larger relative movement

PRACTICAL APPLICATION

The practical application of the work presented in this paper can be illustrated with an example Consider a bridge abutment founded on 400-m-diameter reinforced concrete piles The spacing between individual piles is such that group effects are minimal and can be disregarded The site is underlain by a potentially liquefiable deposit of loose alluvial sands, with an average thickness of about 7.0 m This deposit is susceptible to lateral spread

The mechanical properties of the piles are

Concrete compressive strength	27 6 MPa
Yield stress of reinforcement	413 4 MPa
Longitudinal Reinforcement	10 bars No 4
Diameter of reinforcing cage	300 mm

The piles penetrate the 7-m-thick stratum of potentially liquefiable sand into an end-bearing stratum of dense gravel, and the water table is at the ground surface The coefficient of lateral subgrade reaction of the submerged loose sand is about 1 4 MN/m^3 The axial load acting on each pile is estimated as 300 kN

Cracking and ultimate moments and curvatures for an axial load of 300 kN are

M_c = 19 2 kN-m $\Psi_c = 5\ 145 \times 10^{-4}$

M_u = 117 6 kN-m $\Psi_u = 3\ 270 \times 10^{-2}$

The initial bending stiffness, $(EI)_o$, is 37 2 MN-m^2, while the secant stiffness, $(EI)_{70}$ is about 1157 kN-m^2

Assuming a reduction factor of $R_f = 50$ for the stiffness of the liquefiable layer, the characteristic length of the soil-pile system, $\beta_o H_L$, is about 0 92 According to Figure 13, these conditions would result in soil flow The load coefficient for flow condition is about 1 0, which results in a flow load of 759 kN to induced buckling Therefore, the factor of safety against buckling under soil flow conditions 759/300, or 2 53 These results were duplicated with the computer program B-STRUCT The numerical results indicate that the induced pile deflection at the pile top due to soil flow is about 38 mm

CONCLUDING REMARKS

This paper describes an analytical approach to evaluate the response of single piles and pile groups to horizontal ground displacements caused by soil liquefaction. The analytical model is implemented in a computer program called B-STRUCT The program has been validated against benchmark problems and by comparing numerical predictions with observed pile foundation damage resulting from lateral spread during earthquakes

Three failure mechanisms, excessive bending, buckling, and soil flow, are recognized under lateral spread conditions Each is a function of the relative stiffness between soil and pile, and the axial load carried by the pile At high relative stiffness, piles may fail by excessive bending With decreasing relative stiffness, a soil flow condition may develop in which the liquefied soil flows around the pile without inducing additional pile deflections This mode of pile response is considered safe and provides the basis for acceptable design against structural failure

Buckling may develop as a result of lateral pile displacement and reduced soil stiffness As the relative stiffness of soil to pile increases, the buckling load increases and the failure mode of the pile becomes one of excessive bending Analytical results are combined to develop dimensionless plots which allow for the determination of failure mechanisms on the basis of relative stiffness and applied axial load For the first time, these results show quantitatively how the behavior of deep foundations changes as the ground alters its force-displacement characteristics from a soil-like to a fluid-like medium Dimensionless plots also are developed to determine surface soil displacement required to induce the formation of a plastic hinge under conditions when the axial pile load does not lead to buckling

ACKNOWLEDGMENTS

The research represented in this paper was supported by the National Center for Earthquake Engineering at Buffalo, NY Thanks are extended to Professor F Miura of Yamaguchi University and Dr. T. Miyasaka of the Daido Concrete Company for providing information on reinforced concrete piles K.J Stewart prepared the manuscript, and A. Avcisoy drafted the figures.

REFERENCES

Boresi, A P , Sidebottom, O.M , Seeley, F.B., and Smith, J.O., Advanced Mechanics of Materials, 3rd Ed., John Wiley & Sons, New York, NY, 1978.

Hamada, M , "Large Ground Deformations and Their Effects on Lifelines: 1964 Niigata Earthquake," Case Studies of Liquefaction and Lifeline Performance During Past Earthquakes, Vol. 1, Japanese Case Studies, Technical Report NCEER-92-0001, NCEER, Buffalo, NY, Feb 1992.

Hamada, M., Yasuda, S , Isoyama, R., and Emoto, K , "Study on Liquefaction-Induced Permanent Ground Displacements," Association for the Development of Earthquake Prediction, Tokyo, Japan, Nov. 1986.

Hansen, J.B , "The Ultimate Resistance of Rigid Piles Against Transversal Forces," Report 12, Danish Geotechnical Institute, Copenhagen, 1961, pp. 5-9.

Kent, D C. and Park, R., "Flexural Members with Confined Concrete," Journal of the Structural Division, ASCE, Vol. 97, No. ST7, July 1971, pp 1969-1990

Mander, J.B , Priestley, M.J N., and Park, R , "Theoretical Stress-Strain Model for Confined Concrete," Journal of Structural Engineering, ASCE, Vol. 114, No 8, Aug. 1988, pp 1804-1826.

Marzouk, H. And Chen, Z , "Tension Stiffening Model for High Strength Slabs," Proceedings, 1993 CSCE/CPCA Structural Concrete Conference, Toronto, Canada, May 1993, pp 127-140

Meyersohn, W D., "Pile Response to Liquefaction-Induced Lateral Spread," Ph D Thesis, Cornell University, Ithaca, NY, Jan. 1994.

Meyersohn, W D., O'Rourke, T.D , and Miura, F , "Lateral Spread Effects on Reinforced Concrete Pile Foundations," PWRI Technical Memorandum No 3198, U.S -Japan Workshop on Earthquake Disaster Prevention for Lifeline Systems, Public Works Research Institute, Tsukuba Sience City, Japan, Oct 1992, pp 173-193

Mier, J.G.M. van, "Examples of Non-Linear Analysis of Reinforced Concrete Structures with DIANA," HERON, Delft University of Technology, Delft, Netherlands, Vol 22, No. 3, 1987.

Miura, F and O'Rourke, T.D , "Nonlinear Analysis of Piles Subjected to Liquefaction-Induced Large Ground Deformation," 3rd U S.-Japan Workshop on Earthquake-Resistant Design of Lifeline Facilities and Countermeasures for Soil Liquefaction, Technical Report NCEER-91-0001, NCEER, Buffalo, NY, Feb. 1991, pp 497-512.

Terzaghi, K., "Evaluation of Coefficients of Subgrade Reaction," Geotechnique, Vol 4, No. 4, Dec. 1955, pp 297-326.

Yoshida, N. And Hamada, M , "Damage to Foundation Piles and Deformation Pattern of Ground Due to Liquefaction-Induced Permanent Ground Deformations," 3rd U.S -Japan Workshop on Earthquake-Resistant Design of Lifeline Facilities and Countermeasures for Soil Liquefaction, Technical Report NCEER-91-0001, NCEER, Buffalo, NY, Feb 1991, pp. 147-161